HHS Public Access

Author manuscript

Biomaterials. Author manuscript; available in PMC 2017 September 01.

Published in final edited form as:

Biomaterials. 2016 September ; 102: 220–230. doi:10.1016/j.biomaterials.2016.06.025.

Comparative Biology of Decellularized Lung Matrix: Implications of Species Mismatch in Regenerative Medicine

Jenna L. Balestrini[1,2], **Ashley L. Gard**[1], **Kristin A. Gerhold**[3], **Elise C. Wilcox**[1], **Angela Liu**[1], **Jonas Schwan**[1], **Andrew V. Le**[2], **Pavlina Baevova**[2], **Sashka Dimitrievska**[1], **Liping Zhao**[2], **Sumati Sundaram**[2], **Huanxing Sun**[4], **Laure Rittié**[5], **Rachel Dyal**[6], **Tom J. Broekelmann**[7], **Robert P. Mecham**[7], **Martin A. Schwartz**[1,3], **Laura E. Niklason**[1,2], and **Eric S. White**[6]

[1]Department of Biomedical Engineering, Yale University, New Haven, CT

[2]Department of Anesthesiolgy, Yale University, New Haven, CT

[3]Department of Cell Biology, Yale University, New Haven, CT

[4]Department of Internal Medicine, Yale University, New Haven, CT

[5]Department of Dermatology, Washington University St. Louis, St. Louis, MO

[6]Department of Division of Pulmonary and Critical Care Medicine, Washington University St. Louis, St. Louis, MO

[7]Department of Internal Medicine, University of Michigan Medical School Ann Arbor, MI
Departments of Cell Biology and Physiology, Washington University St. Louis, St. Louis, MO

Abstract

Lung engineering is a promising technology, relying on re-seeding of either human or xenographic decellularized matrices with patient-derived pulmonary cells. Little is known about the species-specificity of decellularization in various models of lung regeneration, or if species dependent cell-matrix interactions exist within these systems. Therefore decellularized scaffolds were produced from rat, pig, primate and human lungs, and assessed by measuring residual DNA, mechanical properties, and key matrix proteins (collagen, elastin, glycosaminoglycans). To study intrinsic matrix biologic cues, human endothelial cells were seeded onto acellular slices and analyzed for markers of cell health and inflammation. Despite similar levels of collagen after decellularization, human and primate lungs were stiffer, contained more elastin, and retained fewer glycosaminoglycans than pig or rat lung scaffolds. Human endothelial cells seeded onto human

All correspondence should be sent to: Eric S. White, MD, 3916 TC, SPC 5360, 1500 E. Medical Center Dr., Ann Arbor, MI 48109-5360, USA.

Author Contributions: JB is responsible for performance of experiments, interpretation of data, and writing the manuscript
AG, KAG, EW, AL, JS, AVL, PB, SD, LZ, SS, HS are all responsible for performing experiments.
LR, RD, TB, RM, MS are responsible for performance of experiments and interpretation of data.
LN is responsible for interpreting results and writing the article.
ESW is the PI of the laboratory, oversees the funding of the study, interpretation of results, and writing the article.
All authors have read, edited, and approved the enclosed article for submission.

and primate lung tissue demonstrated less expression of vascular cell adhesion molecule and activation of nuclear factor-κB compared to those seeded onto rodent or porcine tissue. Adhesion of endothelial cells was markedly enhanced on human and primate tissues. Our work suggests that species-dependent biologic cues intrinsic to lung extracellular matrix could have profound effects on attempts at lung regeneration.

Keywords

decellularization; lung tissue engineering; extracellular matrix; bioactivity

Introduction

For patients with end-stage lung disease, lung transplantation can be the only definitive therapy. However, this procedure is accompanied by high morbidity and mortality, is limited by a shortage of suitable donor lungs, and requires life-long immunosuppression (1). Thus, many investigators are looking to lung regeneration as a possible solution to these limitations. The advent and subsequent improvement of decellularization/recellularization protocols has provided a theoretical means for the creation of patient-specific artificial lungs that could address the current donor tissue shortage while potentially alleviating the need for immunosuppressants (2-5).

In order to develop scaffolds for the construction of bioengineered lungs, donated tissues are decellularized using a series of detergents to remove donor DNA and cellular debris. The resulting decellularized scaffolds are not simply inert “organ templates;” rather these systems impart regulatory signals that actively govern fundamental cellular processes such as proliferation and migration (6), induction of metastatic or fibrotic activity (7), response to growth factors (8), and also provide information regulating appropriate location of specific cell constituents within the matrix (9, 10). These extracellular matrix (ECM) regulatory signals are transmitted via biological cues such as ECM composition and organization, mechanical cues such as matrix stiffness or stretch, and through architectural features such as surface topography (11-13). This “biophysical language” is especially important for cells that undergo mechanical loading (e.g., during breathing), reside in interstitial spaces, or are being reintroduced into decellularized tissue scaffold for the purposes of organ regeneration (14). By providing cells with a suitable scaffold that has retained the appropriate matrix signals, it is more likely that cells reseeded into decellularized scaffolds will have a more functional outcome.

Xenographic lung tissue from rodent, porcine and primate sources are often considered as a model of human tissue, although these systems have innate differences in matrix composition and architecture (Supplemental Table 1). Porcine lungs are also regarded as an ideal donor source for xenotransplantation, and considerable amounts of financial resources have been dedicated to building porcine bioengineered lungs for transplantation into human recipients (4, 15-18). Despite recent advancements in eliminating critical xenographic cellular contribution(s) to organ failure, the survival of primate recipients of porcine lungs is less than 5 days (19-21). Therefore, it is likely that in addition to cellular differences in

species, there are other factors in xenographic tissues that could lead to transplantation failure. Surprisingly, there are few studie s dedicated to examining how the innate differences in animal-derived lung ECM impact human cells. Characterizing the species-dependent impact of the decellularization process is a necessary step towards understanding what models are appropriate for informing the construction of human-derived bioengineered lungs. In this work, we first seek to characterize the species-specific responses to decellularization in relevant models of lung regeneration. Secondly we determine whether human cells exhibit species-dependent cell-matrix interactions within these systems.

Materials and Methods

Rat, Pig, Primate, and Human Lung Tissue

Yale University Institutional Animal Care and Use Committee approved all experimental work performed on rat, porcine, and primate animals in this study. All animal care complied with the Guide for the Care and Use of Laboratory Animals. This study utilized lungs from 12 old Sprague Dawley rats (3-6 months old); 6 Yorkshire pigs (18-25 kg); 4 African Green Vervet monkeys (5-8 years old); and 2 Humans (65-68 years old). All animals (rat, pig and primate) were euthanized via intraperitoneal injection of 150 mg/kg sodium pentobarbital (Sigma). All lungs were intravenously pretreated with 500 U/kg heparin (Sigma-Aldrich). Following euthanasia, the lungs were perfused via the right ventricle with PBS containing 50 U/mL heparin and 1 mg/mL sodium nitroprusside (Fluka). For rat and primate lungs, tracheal and pulmonary artery cannulae were inserted and sutured into place to provide access for perfusion and decellularization. For pig lungs, the accessory lobe was dissected away and the lobar bronchus and artery were cannulated. The accessory lobe, which is the smallest of the seven lobes in the pig lung, makes for a convenient model system for decellularization studies due to its size (22-24).

The native human whole lungs were acquired *en bloc* from brain-dead organ donors during transplant organ recovery through a research protocol with Gift of Life Michigan (Ann Arbor, MI). The University of Michigan Institutional Review Board has considered these approaches exempt from oversight as all subjects are deceased upon lung recovery. Human lungs were sent to Yale University within 24hr post-explant. The right middle lobe was dissected from the whole lung, and processed immediately.

All donors were prescreened for lung disease prior to tissue procurement, and only non-smokers were used in this study. After tissue procurement, human lungs were subsequently examined for abnormalities (interstitial matrix deposition, inflammation, retention of lung architecture) prior to inclusion in this study. All cell experiments were preformed on lung tissue slices that were deemed healthy as ascertained by these metrics.

Decellularization

The decellularization process is described previously, with the addition of a benzonase rinse at the end of the decellularization process (24). Briefly, tissues were perfused using a gravity feed at approximately 30-40 cm H_2O pressure. Infusion of decellularization solutions occurred via the vasculature, or via gentle manual flushing of the airway. Immediately

following procurement, the airways were inflated with PBS containing antibiotics (10% penicillin/streptomycin, 4% amphotericin B, 2% gentamicin). Tissues were mounted within a bioreactor for subsequent decellularization steps. A sequence of low concentration detergents and endonuclease (benzonase, Sigma) were applied within a physiological pH range (pH 7-8) at either 4°C or room temperature. The decellularization protocol concluded with a final PBS buffer and benzonase rinse of the lung vasculature and resulted in the generation of decellularized extracellular matrix scaffolds.

Histology and Immunostaining

Randomly sampled areas (n=3-5) from each native and decellularized lung were isolated and fixed with 10% neutral buffered formalin (Sigma) for 4 hours at room temperature. Samples were then stored overnight in 70% ethanol, embedded in paraffin, and sectioned at 5 μm. Tissue slides were stained for hematoxylin and eosin (H&E), Masson's Trichrome staining (Trichrome), or Verhoff's Van Gieson (EVG) as described previously (24). For immunofluorescence, section were blocked with PBS containing 3% BSA and 0.2% Triton X-100 for 45 minutes, and subsequently incubated in primary antibody against PCNA (Abcam, ab29, 1:1000) overnight at 4°C. After washing slides with PBS, secondary antibody (Alexafluor 555) was used at 1:500 dilution for 45 minutes. The slides were visualized using a Leica DMI6000 B fluorescence microscope.

Collagen assay

Hydroxyproline assays were used to quantify collagen content, as previously described (25). Samples were oxidized with chloramine-T, combined with p-dimethylaminobenzaldehyde (Mallinckrodt Baker, Phillipsburg, NJ), and absorbance was measured at a wavelength of 550 nm against a verified hydroxyproline standard curve. The total hydroxyproline was then quantified for each sample, and and a 1:12 w/w ratio of hydroxyproline was used to calculate the collagen amount. Total collagen content was normalized to dry tissue weight.

Elastin assay

Elastin was measured by determining the desmosine crosslinks via an ELISA assay as described previously (26). Briefly, desmosine crosslinks were measured by first lyophilizing the sample, hydrolyzing with 6N HCL for 48 hr, and reconstituting and filtering the tissue through a 0.45 um filter. Total elastin was normalized to dry tissue weight.

Total glycosaminoglycan [GAG] and sulfated GAG assays

Total GAGs (sulfated and unsulfated) were measured using a carbazole assay as previously described (27). Tissues were digested in 50 U/mL papain (Sigma) overnight and carbizole solution (Sigma) was added. Absorption of the samples were read at 550 nm and run against a heparin standard (Sigma). Sulfated GAGs were quantified using the Blyscan GAG assay kit according to manufacturer's instructions (Biocolor) (24). Content of total and sulfated GAGs were normalized to tissue dry weight.

DNA Quantification

DNA was isolated and quantified using a Quant-iT PicoGreen dsDNA assay kit (Invitrogen, Eugene, OR), following manufacturer's instructions (28). DNA content was normalized to dry tissue weight.

Transmission Electron Microscopy (TEM)

TEM imaging was performed as we have previously described (29). Fixation was done using 2% paraformaldehyde and 2.5% glutaraldehyde in 0.2M Sorensen buffer at pH 7.4 for 30min at room temperature and 1hr at 4°C (24). Following dehydration, samples were infiltrated and embedded in Embed-81, polymerized, and sectioned at 70 nm. Sections were stained in uranyl acetate and lead citrate. A JEOL-JEM-1400 transmission electron microscope was used to view the lung sections.

Tensile testing

Native and decellularized lung samples were analyzed using an Instron 5848 as described previously (24, 30). Briefly, nominal 15 × 2 mm (length × width) strips were obtained the distal region of all lung samples (so as not to include major airways and pleura that could dominate mechanical analysis). Tissues were then pre-tared to 0.01 N, cyclically preconditioned for 3 cycles to 15% strain, and pulled until failure at a strain rate of 1%/sec. Tissues were kept hydrated with PBS before and during the mechanical conditioning. Using tissue dimensions, engineering stress and strain were calculated from force and distance from the slope at the linear regions of the curve. The Young's Modulus (E) for the tissue was determined by dividing the engineering stress,σ, by the engineering strain, ε, at low and high levels of deformation.

Western blotting

Lung tissue slices were immunoblotted for total protein analysis as described previously (12). Protein concentration was determined from native cell lysates using a bicinchoninic acid protein assay (Thermo Fisher Scientific, Lafayette, CO). Lysates were denatured, and equal amounts of protein were subjected to SDS-PAGE followed by immunoblotting. Blots were probed with rabbit anti-phospho P65 (Cell Signaling 3033, 1:3000), rabbit anti P65 (Cell Signaling 3034, 1:2000), rabbit anti-VCAM (Abcam ab134047, 1:1000) and mouse anti-GAPDH (Abcam ab135247, 1:2000). HRP-conjugated secondary goat anti-mouse and goat anti-rabbit antibodies (Invitrogen) were detected by enhanced chemiluminescence (SuperSignal™ West Femto, ThermoFisher).

Cell culture

Human VeraVec cells, a modified umbilical cord endothelial cell line (hVera101, Angiocrine Biosciences, New York, USA), were cultured and expanded on tissue culture plastic at 37°C and 5% CO_2. Cells were cultured in Human Complete EC media, consisting of Medium 199 (Hyclone) and supplemented with 50μg/ml Endothelial Cell Supplement (Biomedical Technologies), fetal bovine serum (Hyclone), 1% antibiotic-antimycotic (Invitrogen), 10mM HEPES buffer (Invitrogen), 50μg/ml Heparin (Sigma), and 1% Glutamax (Life Technologies) (31).

Preparation and Recellularization of Decellularized Lung Slices

Tissue slices were generated from decellularized rat, pig, primate, and human lung tissues and were reseeded with human VeraVec cells as described previously (24, 32). Prior use, all human tissues were examined for age-based abnormalities including the deposition of excessive collagen and architectural integrity. All tissues utilized in cell-seeding experiments were deemed free of abnormalities. Decellularized lung tissues were flash-frozen and slices were cut into sections 300 μm thick (Leica Microsystems, Buffalo Grove, IL). One million VeraVec cells were seeded onto each tissue slice and cultured for three days. A subset of the VeraVec seeded rat slices were treated with TNFα (Cell signaling, 8902SC) at a concentration of 10 ng/ml for 16 hours as a positive control for inflammation. Following culture, cell-seeded slices were fixed, processed, and examined for cell attachment, proliferation, and upregulation of inflammatory markers.

Statistics

Data are presented as the mean and standard deviation, and analyzed with GraphPad for Prism (v 6.0). For comparison of multiple groups a one-way ANOVA test with subsequent Sidak's multiple comparison test was utilized. A p-value lower than 0.05 was considered statistically significant.

Results

Characterization of rat, pig, primate and human lungs

Gross visual examination of tissue showed that decellularized lungs retained general pleural integrity, lobular definition, and airway tree, similar to our prior studies (Booth et al. 2012). Histological analysis of human, primate, pig and rat tissues by H&E images revealed that no intact nuclei were visible in the alveolar septae or vasculature after decellularization in any of the species (Fig. 1A-C). The presence of collagen and elastin was confirmed in all species post-decellularization throughout the entirety of the lung (Fig. 1B, in blue, Fig. 1C in purple, and Fig. 2); however, elastin appeared less prevalent in pig tissue (Fig 2). Fibronectin (FN) was present in all species, although did appear somewhat depleted in pig tissue (Fig. E1, available in the online supplemental). TEM demonstrated that the basement membrane for all species remained intact (Fig. 2A-D), with evidence of cell debris retention in parts of all tissues (Fig 2A). The pig tissue and rat tissue exhibited some areas with cellular debris (Fig 2C, D) located on the basement membrane surface.

Quantitative analyses

Total GAGs, sulfated GAGs (sGAGs), elastin, and collagen in decellularized tissues were measured and compared to native levels (Fig. 3A-D, Table E1 and Figure E2 in the online supplement). Due to cellular removal, all decellularized ECM concentrations are artificially elevated, making comparisons of native and decellularized levels challenging. To address this difficulty, matrix components are presented in multiple fashions: graphically in order to compare native and decellularized tissues visually (Figure 3), as a fraction of total ECM (Supplemental Fig. E2), and in absolute values (Table E1). It should be noted that Supplemental Figure E2 is a reflection of the final composition of the tissue; therefore, loss

of one particular matrix component (e.g., total GAGs) will artificially increase the final percentage of other matrix components. The total mass of each matrix component is also reported and compared to native matrix contents (Fig 3, also see Table E2 in the online supplement) so matrix components can be examined without the confounding issue of cell removal.

Total GAGs in native tissue (Fig. 3A) were highest in rat tissue (Table E1) and lowest in human and primate tissue. The final GAG percentage (relative to lung ECM) for native human, primate, pig and rat lung were 25%, 20%, 51% and 61% respectively (Fig. E2). In decellularized tissue, there was a substantial loss of GAG content in human, primate and rat tissue, although due to artificial concentration of tissues the total GAG levels were only significant in rat ($p < 0.05$). Conversely, total GAG content was generally maintained in pig tissue (Fig 3A, Table E1). The final GAG percentage in decellularized human, primate, pig and rat tissue was 11%, 9%, 26%, and 12% (Fig. E2).

Elastin content was significantly enhanced due to decellularization in rat, primate, and human tissues, whereas in pig tissue it was not (Fig 3B). Final elastin fractions in decellularized tissues remained at 30%, primate and rat increased to 26 and 18% respectively, and pig tissue decreased to 13% (Fig E2). Native human lung tissues had the highest initial fraction of elastin (30%, 14%, 15%, 9%, respectively, Fig. E2) and final fraction of elastin post decellularization (30%, 26%, 13%, 18%, respectively, Fig. E2). Native levels of sGAGs were highest in primate and rat tissues (Fig. 3C, Table E1), yet were substantially retained only in decellularized pig and human tissue (Fig. 3C, $p < 0.01$ and Table E2).

Native collagen content was similar in human, pig and rat tissue in terms of quantity (Fig 3D, Table E1) and fraction of dry weight (45%, 34%, and 30% respectively, Figure E2). Rat and pig tissues underwent a concentration of collagen content that was statistically higher than native tissues (Fig 3D). In decellularized tissues, there was a concentration in human, primate, pig and rat collagen (70%, 61%, 65%, and 59%, respectively, Figs. 3D and E2 B) resulting in similar collagen fractions across species.

The decellularization protocol reduced DNA by 90% or greater in all lung tissues (Table E2). Reduction of DNA was 99.8% in human lung, 98.3% in primate lung, 93.4% in pig lung, 90.0% in rat lung. These data are supported by the complete lack of intact nuclear material on H&E (Fig. 1A).

Mechanical Characterization

Uniaxial tensile testing of native tissue showed differences in mechanical properties from the various species in terms of matrix stiffness (modulus), ultimate tensile strength, and the strain level at which it fails (strain failure) (Fig. 4). Decellularized tissue did not differ statistically from native in any species with regard to modulus or UTS ($p > 0.05$). In terms of strain failure, decellularized human, primate, and rat tissue did not differ statistically from native tissue ($p > 0.05$). Decellularized pig tissue did however have a statistically lower strain at failure relative to native conditions ($p < 0.01$).

Endothelial cell culture

Human endothelial cells (ECs) were seeded onto tissue slices at a concentration of 1×10^6 cells/slice for 3 days (Fig. 5). ECs were noted to distribute evenly throughout human and primate tissues, heterogeneously throughout rat tissue and sparsely in porcine tissue. After three days in culture, ECs proliferated significantly better and were more elongated on human tissues than observed on pig and rat tissues (PCNA stain in Fig. 6; proliferation at 80% vs. 59 and 60% respectively $p < 0.001$; elongation at 1.92 versus 1.64 and 1.75, respectively $p < 0.01$). All cells on tissues were more elongated than TCP controls (Fig. 6, $p < 0.01$), yet only cells placed onto human or primate tissues proliferated more than cells cultured on TCP (Fig. 6, $p < 0.01$). Immunoblotting for phosphorylated NF-kB relative to total NF-kB, and for VCAM, showed that pig tissue led to a significantly higher level of inflammatory marker expression in ECs relative to human tissues (Fig. 7). Rat tissues also induced a statistically higher level of phosphorylated NF-kB relative to total NF-kB in human tissues, but not of VCAM (Fig. 7).

Discussion

In addition to providing structural support, the ECM is important in regulating attachment and phenotypic maintenance of resident cells, and can also dictate healthy remodeling, neoplastic behaviors, or fibrotic disease progression in native or engineered organs (33). In this study, we sought to characterize the species-specific impact of decellularization on lung ECM in human and animal sources, and also to determine whether human cells would be differentially impacted by these decellularized systems. Our data show that, despite identical decellularization protocols, there is a species-specific response to the procedure that renders matrices unequal following decellularization, with differences being noted in retention of matrix components, collagen assembly, and mechanical properties. Perhaps more importantly with respect to the application of such matrices for human lung regeneration, we observed striking differences in endothelial cell responses to the various matrices.

Morphology, ECM composition, and mechanical properties of human, primate, pig and rat native lung tissue demonstrated a strong phylogenetic dependency. Specifically, native rat and pig lung tissues are more GAG dense, elastin sparse, and weaker than human and primate tissues (Fig. 3; Fig 4C, E). It is possible that the differences in native ECM content of various species are due, in part, to the whether the animals are quadruped or bipedal, as mode of ambulation impacts breathing mechanics (34). The observed species-dependent lung properties reported in this work corroborate findings in the literature, including differences in alveolar size and septal thickness (35-38); GAG, collagen, and elastin content (17, 39); matrix stiffness (40, 41), and alveolar cellular composition (42, 43).

Our results indicate differential matrix conservation with respect to species. The consequences of specific protein damage or removal can range from impaired cell attachment due the loss of fibronectin, (44), substantial loss of mechanical integrity from loss of collagen type I (45), elastin (15) or GAGs (46), or induction of endothelial inflammation associated with pulmonary disease (47). Further, the preservation of damaged GAGs could render the sequestering of unwanted cellular components.

Of the species tested herein, decellularized human lung retained an ECM profile most closely resembling that of native lung, primate tissue underwent modest changes in matrix composition, and pig and rat tissue demonstrated significant ECM loss. The impact of decellularization on ECM loss in pig lung was different than that observed in other species, resulting in a matrix with the highest percentage of GAG content and lowest percentage of elastin content (~ 30% GAGs, 60% collagen, and 10% elastin). This differential ECM retention and loss resulted in a tissue that was markedly different from human decellularized tissue in terms of composition, mechanical properties and cell-matrix interactions (Figs 3, Fig. 4C, E, and Figs 5-7).

One limitation to our study includes difference in age among our species selected in this work. Lung development varies dramatically across species in terms of both cellular and tissue components, making age-matching of species difficult and somewhat arbitrary. For example, rodents are born with lungs that are at the saccular stage of development and completely lack alveoli, yet the bulk of alveolar development is completed pre-puberty (< 2 months old) (48). Pigs are born with advanced alveolar development that is finalized shortly after birth (49), while the alveolar number and lung structure in non-human primates changes far into adulthood and continues until ~ 10 years of age (50, 51). Finally, it there is insufficient data in the literature for some of our species to know at what age the ECM has matured or is degraded. Although the animals selected in this study were not age matched, the tissues utilized in this work come from lungs of animals where the matrix and cellular constituents were relatively stable in development and free from age-related lung pathology. Furthermore, the age of porcine samples (~ 3 months) was selected based on the size of lungs that could be used as a potential xenographic donor source for human recipients.

Previous studies have indicated that 1) ECM retention after decellularization is higher in younger tissues, and 2) *de novo* matrix production and cell proliferation is increased after recellularization using younger rather than older tissues (52, 53). Taken together, these previous works predict that in the absence of species-specific cell-matrix interactions, our human ECs should perform better on rat and pig (younger) tissues rather than primate and human (older) tissues. On the contrary, our cells attach, elongate, proliferate and elicit reduced inflammatory behavior when seeded on human and primate tissues relative to rat and pig tissues. It is possible that these observations of species preference in ECs would be even more profound on younger human and primate tissue sources.

The results from this study provide some of the first insights into the impact that species-dependent scaffold has on the attachment, elongation, and proliferation of seeded human ECs. Nuclear elongation in ECs has been shown to correlate with increases in cell spreading and proliferation (54). Interestingly, although ECs elongated when seeded onto all decellularized matrix sources (relative to TCP), only cells seeded onto human or primate tissues demonstrated increases in proliferation.

The NF-κB pathway of transcription factors is critical to regulating inflammation, differentiation, proliferation, and apoptosis (55). Expression of phosphorylated p65 observed in human ECs seeded onto decellularized rat and pig matrix is two-fold and four-fold higher, respectively, when compared to that observed on human and primate matrix, suggesting

increased inflammatory activation. VCAM-1, an endothelial cell membrane glycoprotein implicated in leukocyte-endothelial cell interactions in inflammation (56) and downstream transcriptional target of NF-κB, is also expressed at three-fold higher levels in cells seeded onto pig matrix. These results suggest that species mismatch, most noticeably between pig and human, could drive inflammatory behavior in recellularized tissues independent of xenogeneic cellular contributions. This inflammatory activation of the endothelium would render major consequences for vascular permeability and ultimately implant rejection.

Unlike other species, a considerable amount of research has been dedicated towards using pigs as xenogeneic donor sources for lung transplantation into human patients. Complications of porcine lung xenografts use include hyperacute rejections mediated by anti-Gal antibodies; intravascular and alveolar macrophages that produce inflammatory cytokines, amplify procoagulant factors, and phagocytize human blood cells and platelets; and human natural killer cells (NK) that infiltrate pig organs and lyse pig endothelial cells (20, 21, 57). To mitigate these cell-based rejection limitations, research has focused the use of decellularized pig lungs as a potential platform for the construction of engineered lungs (4, 15, 17, 24). In this work, we found both the final composition and arrangement of matrix to be strikingly different between human and pig lungs. Finally and most importantly, human cells seeded onto decellularized pig matrix responded by producing markers of inflammation. Inflammatory activation of the endothelium could have major consequences regarding vascular permeability and ultimately graft rejection (58).

In order for tissue-engineered lungs to be functional, they would at minimum need to 1) provide a barrier to separate blood from air, along with functional alveolar epithelial and microvascular endothelial cells; 2) have a hierarchical branching geometry that provides high surface area for gas exchange, 3) be sufficiently mechanically robust to allow for ventilation and physiological mechanical stresses 4) contain a perfusable microvasculature that is resistant to thrombosis, and 5) maintain lung-specific cells: i.e., cells that produce surfactant, growth factors, have cilia, etc (59). To date, studies by our group and others have demonstrated feasibility of decellularized human, primate, pig and rat tissues in achieving some of these features (5, 18, 24, 29, 60-63). In this work, we demonstrated that the basement membrane (required to separate the blood supply), and the gross tissue architecture needed to provide gas exchange were maintained in each of our decellularized species. We also found that each of our species maintain mechanical integrity post decellularization, although pig tissues demonstrated a lower strain at failure relative to native tissues. Finally, we examined the potential for each of these tissues to maintain human ECs, and found that human cells demonstrated preference of human or primate tissues over rat and pig tissue with respect to attachment, proliferation, and health. Therefore, order to create a healthy, patent vasculature with sufficient endothelial coverage, the donor lung species will require some consideration.

Supplementary Material

Refer to Web version on PubMed Central for supplementary material.

Acknowledgments

Support: The authors would like to thank the Veterinary Care Services at Yale for their invaluable technical assistance and Matthew Lawrence for his generous donation of primate lungs. This work was supported by HL111016-01 (to L.E.N and E.S.W.), HL75092 (to M.A.S.), and HL105314 (to R.P.M). L.E.N. has a financial interest in Humacyte, Inc, a regenerative medicine company. Humacyte did not fund these studies, and Humacyte did not affect the design, interpretation, or reporting of any of the experiments herein.

References

1. Yusen RD, Edwards LB, Kucheryavaya AY, Benden C, Dipchand AI, Dobbels F, Goldfarb SB, Levvey BJ, Lund LH, Meiser B, Stehlik J. International Society for H, Lung T. The registry of the International Society for Heart and Lung Transplantation: thirty-first adult lung and heart-lung transplant report--2014; focus theme: retransplantation. J Heart Lung Transplant. 2014; 33:1009–1024. [PubMed: 25242125]
2. Ott HC, Clippinger B, Conrad C, Schuetz C, Pomerantseva I, Ikonomou L, Kotton D, Vacanti JP. Regeneration and orthotopic transplantation of a bioartificial lung. Nat Med. 2010; 16:927–933. [PubMed: 20628374]
3. Price AP, England KA, Matson AM, Blazar BR, Panoskaltsis-Mortari A. Development of a Decellularized Lung Bioreactor System for Bioengineering the Lung: The Matrix Reloaded. Tissue Eng Part A. 2010; 16:2581–2591. [PubMed: 20297903]
4. Nichols JE, Niles J, Riddle M, Vargas G, Schilagard T, Ma L, Edward K, La Francesca S, Sakamoto J, Vega S, Ogadegbe M, Mlcak R, Deyo D, Woodson L, McQuitty C, Lick S, Beckles D, Melo E, Cortiella J. Production and assessment of decellularized pig and human lung scaffolds. Tissue Eng Part A. 2013; 19:2045–2062. [PubMed: 23638920]
5. Bonvillain RW, Danchuk S, Sullivan DE, Betancourt AM, Semon JA, Eagle ME, Mayeux JP, Gregory AN, Wang G, Townley IK, Borg ZD, Weiss DJ, Bunnell BA. A nonhuman primate model of lung regeneration: detergent-mediated decellularization and initial in vitro recellularization with mesenchymal stem cells. Tissue Eng Part A. 2012; 18:2437–2452. [PubMed: 22764775]
6. Vorotnikova E, McIntosh D, Dewilde A, Zhang J, Reing JE, Zhang L, Cordero K, Bedelbaeva K, Gourevitch D, Heber-Katz E, Badylak SF, Braunhut SJ. Extracellular matrix-derived products modulate endothelial and progenitor cell migration and proliferation in vitro and stimulate regenerative healing in vivo. Matrix Biol. 2010; 29:690–700. [PubMed: 20797438]
7. Murray JC, Liotta L, Rennard SI, Martin GR. Adhesion characteristics of murine metastatic and nonmetastatic tumor cells in vitro. Cancer Res. 1980; 40:347–351. [PubMed: 7356518]
8. Clark RA, Nielsen LD, Welch MP, McPherson JM. Collagen matrices attenuate the collagen-synthetic response of cultured fibroblasts to TGF-beta. J Cell Sci. 1995; 108(Pt 3):1251–1261. [PubMed: 7622608]
9. Crapo PM, Medberry CJ, Reing JE, Tottey S, van der Merwe Y, Jones KE, Badylak SF. Biologic scaffolds composed of central nervous system extracellular matrix. Biomaterials. 2012; 33:3539–3547. [PubMed: 22341938]
10. Reing JE, Brown BN, Daly KA, Freund JM, Gilbert TW, Hsiong SX, Huber A, Kullas KE, Tottey S, Wolf MT, Badylak SF. The effects of processing methods upon mechanical and biologic properties of porcine dermal extracellular matrix scaffolds. Biomaterials. 2010; 31:8626–8633. [PubMed: 20728934]
11. Balestrini JL, Billiar KL. Magnitude and duration of stretch modulate fibroblast remodeling. J Biomech Eng. 2009; 131:051005. [PubMed: 19388775]
12. Balestrini JL, Chaudhry S, Sarrazy V, Koehler A, Hinz B. The mechanical memory of lung myofibroblasts. Integr Biol (Camb). 2012; 4:410–421. [PubMed: 22410748]
13. Padmanabhan P, Radhakrishnan A, Venkataraman AP, Gupta N, Srinivasan B. Corneal changes following collagen cross linking and simultaneous topography guided photoablation with collagen cross linking for keratoconus. Indian J Ophthalmol. 2014; 62:229–235. [PubMed: 23619500]
14. Balestrini JL, Niklason LE. Extracellular Matrix as a Driver for Lung Regeneration. Ann Biomed Eng. 2014

15. O'Neill JD, Anfang R, Anandappa A, Costa J, Javidfar J, Wobma HM, Singh G, Freytes DO, Bacchetta MD, Sonett JR, Vunjak-Novakovic G. Decellularization of human and porcine lung tissues for pulmonary tissue engineering. Ann Thorac Surg. 2013; 96:1046–1055. discussion 1055-1046. [PubMed: 23870827]
16. Wagner DE, Bonenfant NR, Sokocevic D, DeSarno MJ, Borg ZD, Parsons CS, Brooks EM, Platz JJ, Khalpey ZI, Hoganson DM, Deng B, Lam YW, Oldinski RA, Ashikaga T, Weiss DJ. Three-dimensional scaffolds of acellular human and porcine lungs for high throughput studies of lung disease and regeneration. Biomaterials. 2014; 35:2664–2679. [PubMed: 24411675]
17. Gilpin SE, Guyette JP, Gonzalez G, Ren X, Asara JM, Mathisen DJ, Vacanti JP, Ott HC. Perfusion decellularization of human and porcine lungs: bringing the matrix to clinical scale. J Heart Lung Transplant. 2014; 33:298–308. [PubMed: 24365767]
18. Price AP, Godin LM, Domek A, Cotter T, D'Cunha J, Taylor DA, Panoskaltsis-Mortari A. Automated decellularization of intact, human-sized lungs for tissue engineering. Tissue Eng Part C Methods. 2015; 21:94–103. [PubMed: 24826875]
19. Cantu E, Balsara KR, Li B, Lau C, Gibson S, Wyse A, Baig K, Gaca J, Gonzalez-Stawinski GV, Nichols T, Parker W, Davis RD. Prolonged function of macrophage, von Willebrand factor-deficient porcine pulmonary xenografts. Am J Transplant. 2007; 7:66–75. [PubMed: 17109734]
20. Nguyen BN, Azimzadeh AM, Zhang T, Wu G, Schuurman HJ, Sachs DH, Ayares D, Allan JS, Pierson RN 3rd. Life-supporting function of genetically modified swine lungs in baboons. J Thorac Cardiovasc Surg. 2007; 133:1354–1363. [PubMed: 17467457]
21. Nguyen BN, Azimzadeh AM, Schroeder C, Buddensick T, Zhang T, Laaris A, Cochrane M, Schuurman HJ, Sachs DH, Allan JS, Pierson RN 3rd. Absence of Gal epitope prolongs survival of swine lungs in an ex vivo model of hyperacute rejection. Xenotransplantation. 2011; 18:94–107. [PubMed: 21496117]
22. Stahl WR. Scaling of respiratory variables in mammals. J Appl Physiol. 1967; 22:453–460. [PubMed: 6020227]
23. Tillery SI, Lehnert BE. Age-bodyweight relationships to lung growth in the F344 rat as indexed by lung weight measurements. Lab Anim. 1986; 20:189–194. [PubMed: 3795855]
24. Balestrini JL, Gard AL, Leiby KL, Calle E, Sivarapatna A, Kunkemoeller B, Lin T, Dimitrievska S, Niklason LE. Production of decellularized porcine lung scaffolds for use in tissue engineering. Integrative Biology. 2015
25. Woessner JF, Boucek RJ. Connective Tissue Development in Subcutaneously Implanted Polyvinyl Sponge. Archives of Biochemistry and Biophysics. 1961; 93:85–94. [PubMed: 13786178]
26. Swaminathan G, Gadepalli VS, Stoilov I, Mecham RP, Rao RR, Ramamurthi A. Pro-elastogenic effects of bone marrow mesenchymal stem cell-derived smooth muscle cells on cultured aneurysmal smooth muscle cells. J Tissue Eng Regen Med. 2014
27. Warda M, Gouda EM, Toida T, Chi L, Linhardt RJ. Isolation and characterization of raw heparin from dromedary intestine: evaluation of a new source of pharmaceutical heparin. Comp Biochem Physiol C Toxicol Pharmacol. 2003; 136:357–365. [PubMed: 15012907]
28. Tsuchiya T, Balestrini JL, Mendez J, Calle EA, Zhao L, Niklason LE. Influence of pH on extracellular matrix preservation during lung decellularization. Tissue Eng Part C Methods. 2014; 20:1028–1036. [PubMed: 24735501]
29. Booth AJ, Hadley R, Cornett AM, Dreffs AA, Matthes SA, Tsui JL, Weiss K, Horowitz JC, Fiore VF, Barker TH, Moore BB, Martinez FJ, Niklason LE, White ES. Acellular normal and fibrotic human lung matrices as a culture system for in vitro investigation. Am J Respir Crit Care Med. 2012; 186:866–876. [PubMed: 22936357]
30. Dimitrievska S, Cai C, Weyers A, Balestrini JL, Lin T, Sundaram S, Hatachi G, Spiegel DA, Kyriakides TR, Miao J, Li G, Niklason LE, Linhardt RJ. Click-coated, heparinized, decellularized vascular grafts. Acta Biomater. 2015; 13:177–187. [PubMed: 25463496]
31. Balestrini JL, Gard AL, Liu A, Leiby KL, Schwan J, Kunkemoeller B, Calle EA, Sivarapatna A, Lin T, Dimitrievska S, Cambpell SG, Niklason LE. Production of decellularized porcine lung scaffolds for use in tissue engineering. Integr Biol (Camb). 2015

32. Balestrini JL, Liu A, Gard AL, Huie JL, Blatt KM, Schwan J, Broekelmann T, Mecham R, Wilcox EC, Zhao L, Niklason L. Sterilization of Lung Matrices by Supercritical Carbon Dioxide. Tissue Eng Part C Methods. 2015
33. Hynes RO. The extracellular matrix: not just pretty fibrils. Science. 2009; 326:1216–1219. [PubMed: 19965464]
34. Hsia CC, Schmitz A, Lambertz M, Perry SF, Maina JN. Evolution of air breathing: oxygen homeostasis and the transitions from water to land and sky. Compr Physiol. 2013; 3:849–915. [PubMed: 23720333]
35. Section 3- Selected Biological Properties of Tissues: Potential Determinants of Susceptibility to Ultrasound-Induced Bioeffects. Journal of ultrasound in medicine: official journal of the American Institute of Ultrasound in Medicine. 2000; 19:85–168. [PubMed: 10680615]
36. Mercer RR, Russell ML, Crapo JD. Alveolar septal structure in different species. J Appl Physiol (1985). 1994; 77:1060–1066. [PubMed: 7836104]
37. Hoyt, JR.; Hawkins, JV.; St Clair, MB.; Kennett, MJ. The Mouse in Biomedical Research: Normative Biology, Husbandry, and Models Burlington. Massachusetts: Academic Press; 2006.
38. Mansell AL, Collins MH, Johnson E Jr, Gil J. Postnatal growth of lung parenchyma in the piglet: morphometry correlated with mechanics. Anat Rec. 1995; 241:99–104. [PubMed: 7879927]
39. Starcher BC. Elastin and the lung. Thorax. 1986; 41:577–585. [PubMed: 3538485]
40. Salerno FG, Ludwig MS. Elastic moduli of excised constricted rat lungs. J Appl Physiol. 1999; 86:66–70. [PubMed: 9887114]
41. Liu F, Tschumperlin DJ. Micro-mechanical characterization of lung tissue using atomic force microscopy. J Vis Exp. 2011
42. Crapo JD, Barry BE, Gehr P, Bachofen M, Weibel ER. Cell number and cell characteristics of the normal human lung. Am Rev Respir Dis. 1982; 126:332–337. [PubMed: 7103258]
43. Pinkerton KE, Gehr P, Crapo JD. Architecture and cellular composition of the air-blood barrier. Comparative Biology of the Normal Lung. 1992; 1:121–128.
44. Tsukahara H, Noiri E, Jiang MZ, Hiraoka M, Mayumi M. Role of nitric oxide in human pulmonary microvascular endothelial cell adhesion. Life Sci. 2000; 67:1–11. [PubMed: 10896023]
45. Petersen TH, Calle EA, Colehour MB, Niklason LE. Matrix composition and mechanics of decellularized lung scaffolds. Cells Tissues Organs. 2012; 195:222–231. [PubMed: 21502745]
46. Al Jamal R, Roughley PJ, Ludwig MS. Effect of glycosaminoglycan degradation on lung tissue viscoelasticity. Am J Physiol Lung Cell Mol Physiol. 2001; 280:L306–315. [PubMed: 11159010]
47. Houghton AM, Quintero PA, Perkins DL, Kobayashi DK, Kelley DG, Marconcini LA, Mecham RP, Senior RM, Shapiro SD. Elastin fragments drive disease progression in a murine model of emphysema. J Clin Invest. 2006; 116:753–759. [PubMed: 16470245]
48. Massaro D, Teich N, Maxwell S, Massaro GD, Whitney P. Postnatal development of alveoli. Regulation and evidence for a critical period in rats. J Clin Invest. 1985; 76:1297–1305. [PubMed: 4056033]
49. Winkler GC, Cheville NF. Morphometry of postnatal development in the porcine lung. Anat Rec. 1985; 211:427–433. [PubMed: 3993992]
50. Hyde DM, Robinson NE, Gillespie JR, Tyler WS. Morphometry of the distal air spaces in lungs of aging dogs. J Appl Physiol Respir Environ Exerc Physiol. 1977; 43:86–91. [PubMed: 893271]
51. Shimura S, Boatman ES, Martin CJ. Effects of ageing on the alveolar pores of Kohn and on the cytoplasmic components of alveolar type II cells in monkey lungs. J Pathol. 1986; 148:1–11. [PubMed: 3944670]
52. Sokocevic D, Bonenfant NR, Wagner DE, Borg ZD, Lathrop MJ, Lam YW, Deng B, Desarno MJ, Ashikaga T, Loi R, Hoffman AM, Weiss DJ. The effect of age and emphysematous and fibrotic injury on the re-cellularization of de-cellularized lungs. Biomaterials. 2013; 34:3256–3269. [PubMed: 23384794]
53. Godin LM, Sandri BJ, Wagner DE, Meyer CM, Price AP, Akinnola I, Weiss DJ, Panoskaltsis-Mortari A. Decreased Laminin Expression by Human Lung Epithelial Cells and Fibroblasts Cultured in Acellular Lung Scaffolds from Aged Mice. PLoS One. 2016; 11:e0150966. [PubMed: 26954258]

54. Versaevel M, Grevesse T, Gabriele S. Spatial coordination between cell and nuclear shape within micropatterned endothelial cells. Nat Commun. 2012; 3:671. [PubMed: 22334074]
55. Orr AW, Hahn C, Blackman BR, Schwartz MA. p21-activated kinase signaling regulates oxidant-dependent NF-kappa B activation by flow. Circ Res. 2008; 103:671–679. [PubMed: 18669917]
56. Wong D, Dorovini-Zis K. Expression of vascular cell adhesion molecule-1 (VCAM-1) by human brain microvessel endothelial cells in primary culture. Microvasc Res. 1995; 49:325–339. [PubMed: 7543972]
57. Kubicki N, Laird C, Burdorf L, Pierson RN 3rd, Azimzadeh AM. Current status of pig lung xenotransplantation. Int J Surg. 2015
58. Tible M, Loupy A, Vernerey D, Suberbielle C, Beuscart T, Cazes A, Guillemain R, Amrein C, Pezzella V, Fabiani JN, Nochy D, Hill G, Empana JP, Jouven X, Charron D, Bruneval P, Duong Van Huyen JP. Pathologic classification of antibody-mediated rejection correlates with donor-specific antibodies and endothelial cell activation. J Heart Lung Transplant. 2013; 32:769–776. [PubMed: 23856214]
59. Calle EA, Ghaedi M, Sundaram S, Sivarapatna A, Tseng MK, Niklason LE. Strategies for whole lung tissue engineering. IEEE Trans Biomed Eng. 2014; 61:1482–1496. [PubMed: 24691527]
60. Petersen TH, Calle EA, Zhao L, Lee EJ, Gui L, Raredon MB, Gavrilov K, Yi T, Zhuang ZW, Breuer C, Herzog E, Niklason LE. Tissue-engineered lungs for in vivo implantation. Science. 2010; 329:538–541. [PubMed: 20576850]
61. Gilpin SE, Ott HC. Using nature's platform to engineer bio-artificial lungs. Annals of the American Thoracic Society. 2015; 12(1):S45–49. [PubMed: 25830835]
62. Wagner DE, Bonenfant NR, Parsons CS, Sokocevic D, Brooks EM, Borg ZD, Lathrop MJ, Wallis JD, Daly AB, Lam YW, Deng B, Desarno MJ, Ashikaga T, Loi R, Weiss DJ. Comparative decellularization and recellularization of normal versus emphysematous human lungs. Biomaterials. 2014; 35:3281–3297. [PubMed: 24461327]
63. Zvarova B, Uhl FE, Uriarte JJ, Borg ZD, Coffey AL, Bonenfant NR, Weiss DJ, Wagner DE. Residual Detergent Detection Method for Non-Destructive Cytocompatibility Evaluation of Decellularized Whole Lung Scaffolds. Tissue Eng Part C Methods. 2016

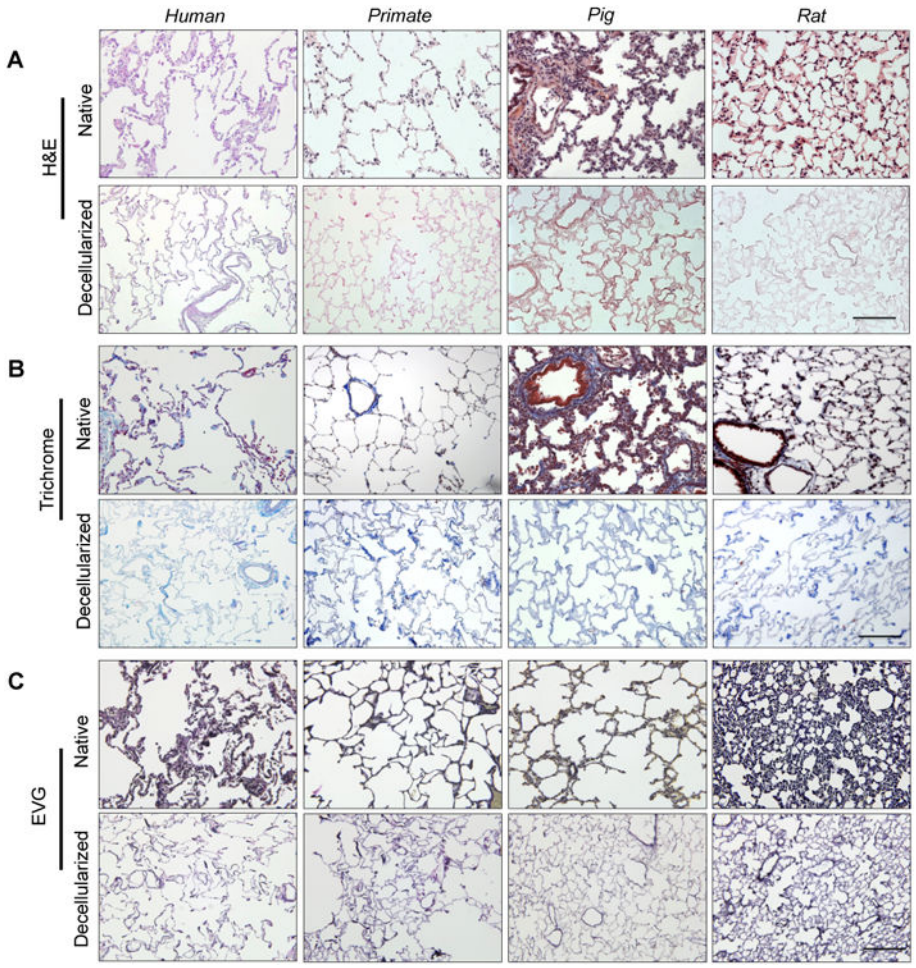

Fig. 1. Characterization of human, primate, pig and rat decellularized lung matrix

(A) Representative native and decellularized lung tissue, as visualized by hematoxylin and eosin (H&E). Sections indicate maintenance of tissue architecture, removal of debris and blood, and lack of visible nuclear material. B) Preservation of collagen (blue) is visualized using Masson's Trichrome, and C) elastin (blue-black) by Verhoeff-Van Gieson staining. Scale bar = 100 μm applies to all panels.

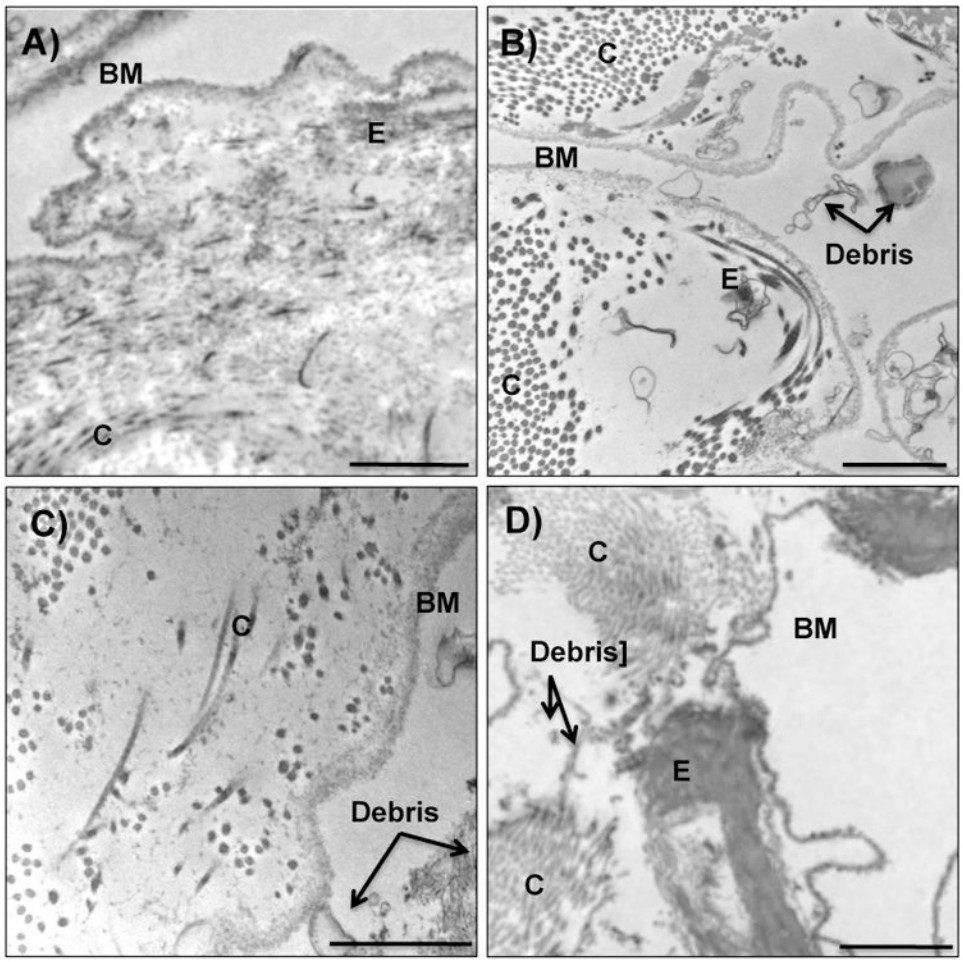

Figure 2. TEM images of decellularized tissue

Representative transmission electron micrographs of A) human, B) primate, C) pig and D) rat decellularized tissue. Irrespective of species, decellularized lungs appeared to lack intact cellular bodies and retain basement membranes and characteristic normal architecture. Of the species tested, human decellularized tissue demonstrated the greatest homogeneous clearing of cellular debris. Collagen content appeared in clusters throughout the entirety of the primate lungs, and dispersed more sporadically throughout rat, pig and human tissue. Elastin did not appear highly concentrated in porcine tissue. Basement membrane (BM), collagen (C), elastin (E), and cellular debris (debris) are indicated with black arrows. Scale bar = 1 μm.

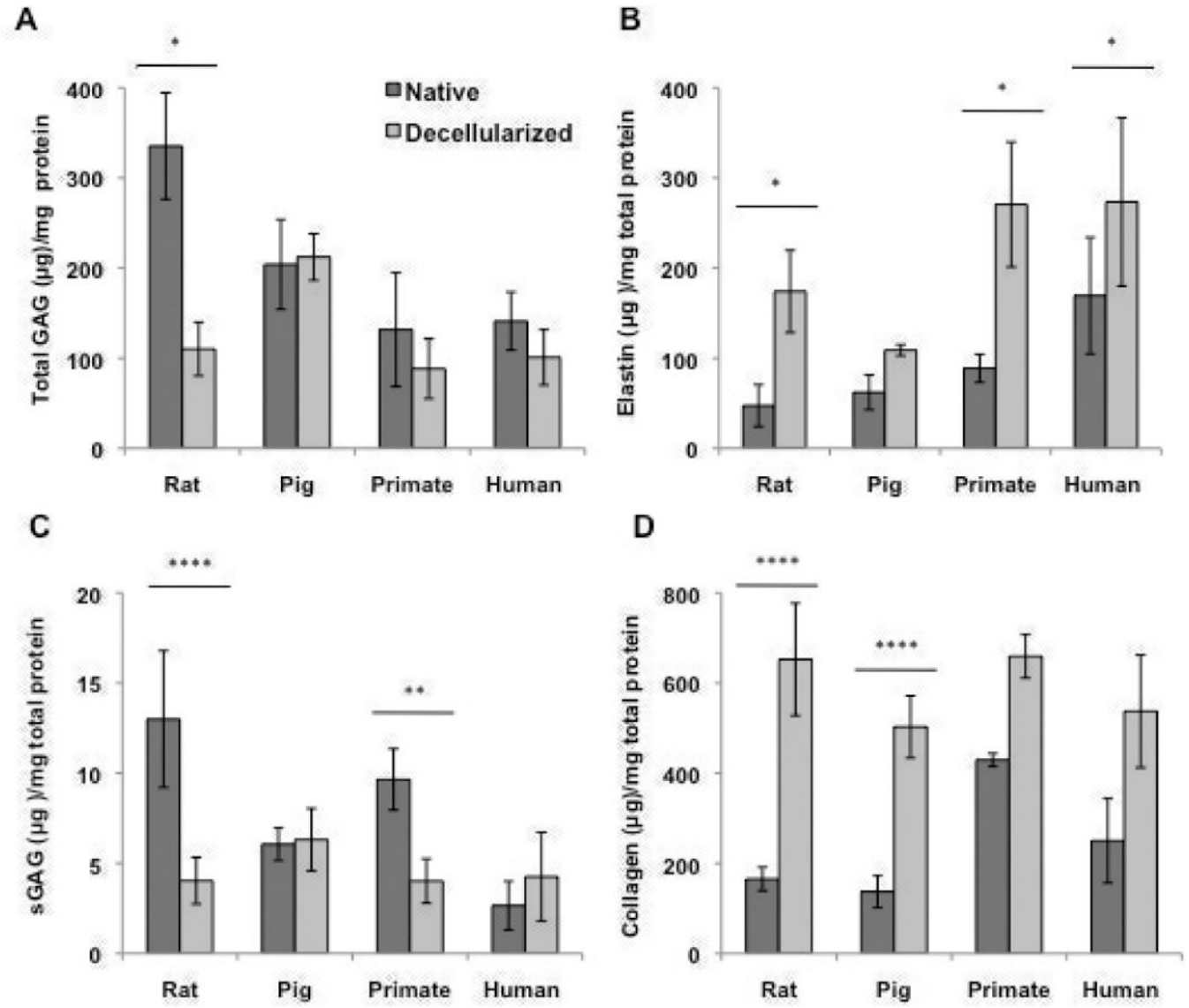

Figure 3. Matrix analyses of rat, porcine, primate and human decellularized lung tissue

Quantification of A) Total GAGs, B) elastin content, C) sGAGs, and D) collagen content of native and decellularized indicate the retention or loss of matrix post decellularization. For all ECM analysis, 3-5 pieces per lung were utilized and averaged (n=3, 3, 4, and 2 for rat, porcine, primate and human native and decellularized tissue). Quantitative values all normalized to dry starting tissue weight. * indicates $p \leq 0.05$, ** $p \leq 0.01$, *** $p \leq 0.001$, and **** $p \leq 0.0001$.

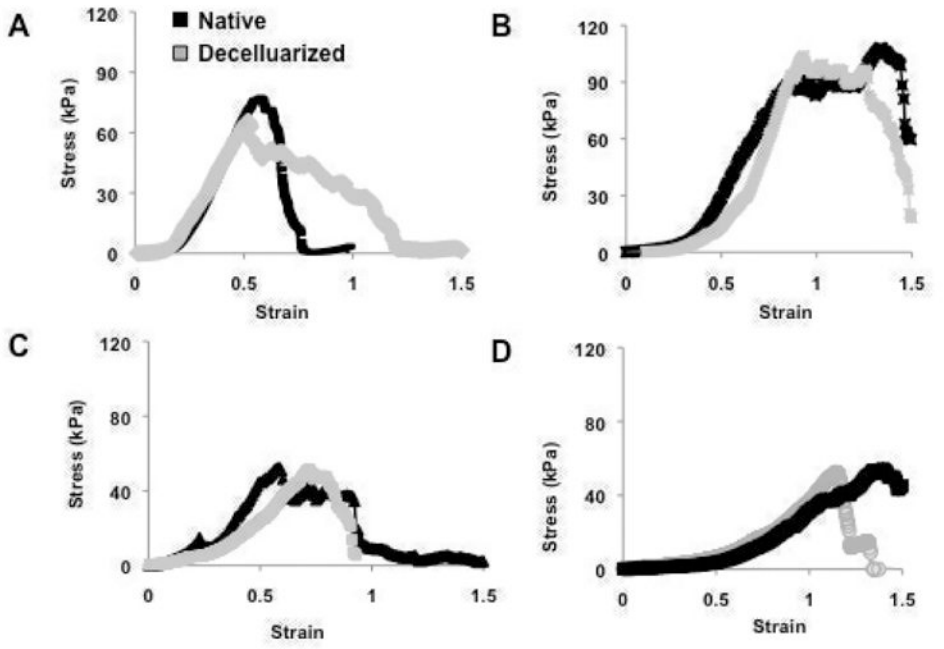

		Human	Primate	Pig	Rat
Modulus (kPa)	*Native*	9.6 ± 1.9	7.6 ± 3.0	6.4 ± 2.3	3.6 ± 1.0
	Decell	7.7 ± 2.8	4.8 ± 0.7	7.3 ± 2.3	4.1 ± 0.8
UTS (kPa)	*Native*	67.3 ± 12.3	99.3 ± 25.1	42.2 ± 10.7	32.9 ± 3.0
	Decell	63.8 ± 1.6	100.3 ± 4.4	37.1 ± 9.5	34.5 ± 5.8
Strain at Failure (%)	*Native*	107.0 ± 19.4	142.9 ± 26.4	177.8 ± 17.7	135.7 ± 18.4
	Decell	97.0 ± 31.4	180.8 ± 40.9	112.6 ± 30.8**	126.0 ± 19.1

Fig 4. Mechanical analysis of decellularized matrix

Representative stress strain curves of A) human, B) primate, C) pig, and D) rat native and decellularized tissue. B) Modulus, UTS, and Strain at Failure for native and decellularized lung tissue. ** indicates significance from native tissue at $p \leq 0.01$.

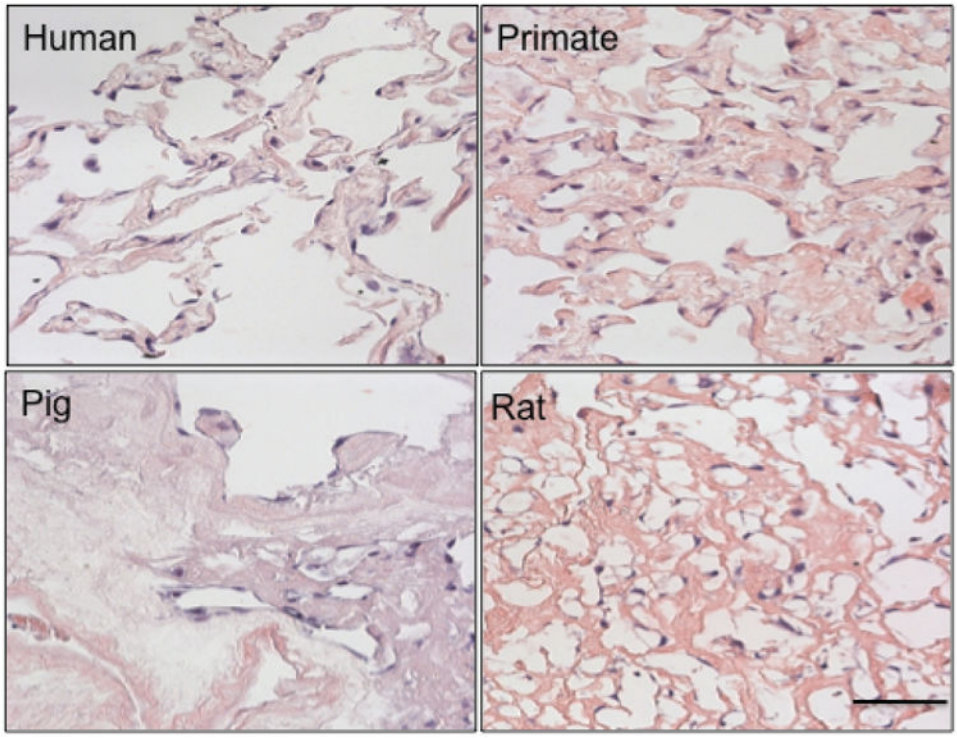

Fig. 5. Endothelial cell engraftment is species dependent

Human endothelial cells were seeded onto 1 cm^2 tissue slices at a concentration of 1×10^6 cells/slice for 3 days. Cells homogenously attached in both the primate and human tissue, heterogeneously throughout the rat tissue, and sparsely through the pig tissue. Scale bar = 100 μm applies to all panels.

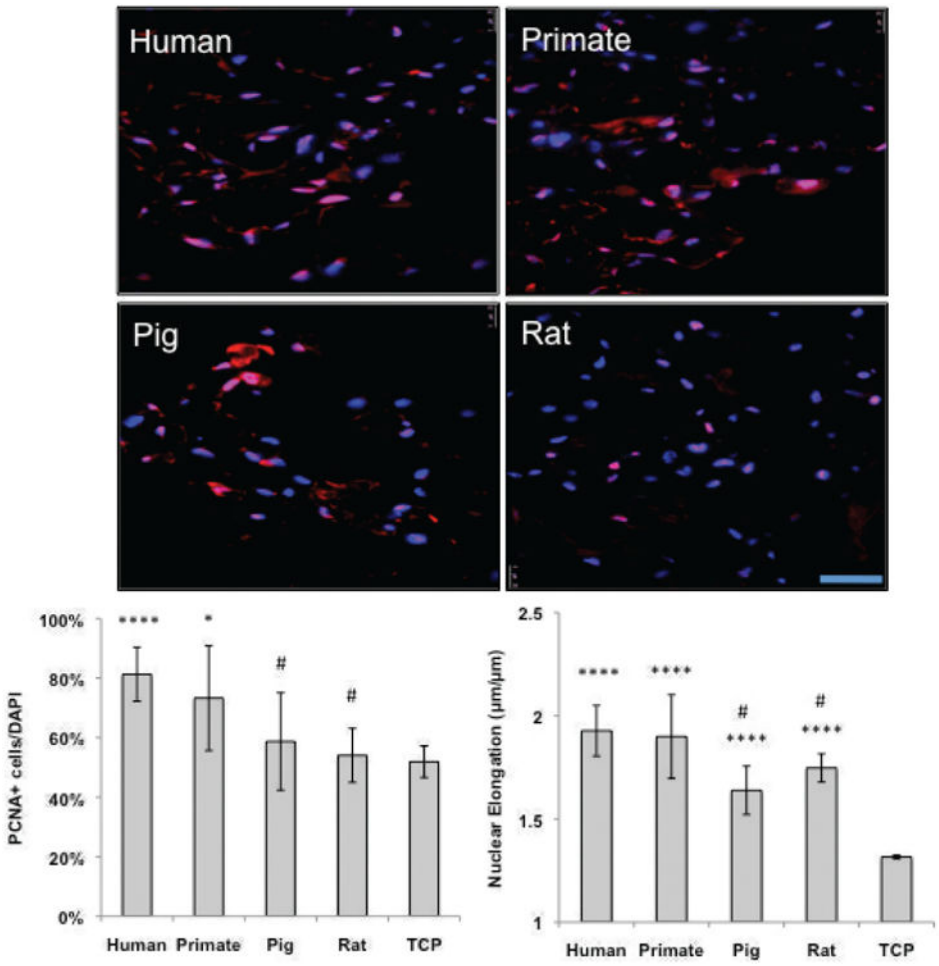

Fig. 6. Human endothelial cells demonstrate enhanced proliferation on human and primate matrix

Representative IF images of reseeded decellularized human, primate, pig and rat tissue. Human endothelial (VeraVec) cells were seeded onto 1 cm^2 tissue slices at a concentration of 1,000,000 cells/slice for 3 days and stained for DAPI (in blue) PCNA (in red). The percentage positive cells (PCNA/DAPI) are noted in the bottom right hand of the images (n=4, average of 10 images). All cells on tissue were significantly more elongated than cells on TCP, yet only cells on human and primate tissues proliferated more than on TCP. Human cells proliferated significantly higher and were more elongated on human and primate tissue than on pig and rat tissues. Scale bar = 100 μm applies to all panels. * indicates $p \leq 0.05$, ** $p \leq 0.01$, *** $p \leq 0.001$, and **** $p \leq 0.0001$ relative to TCP, # indicates $p \leq 0.05$ relative to human tissues.

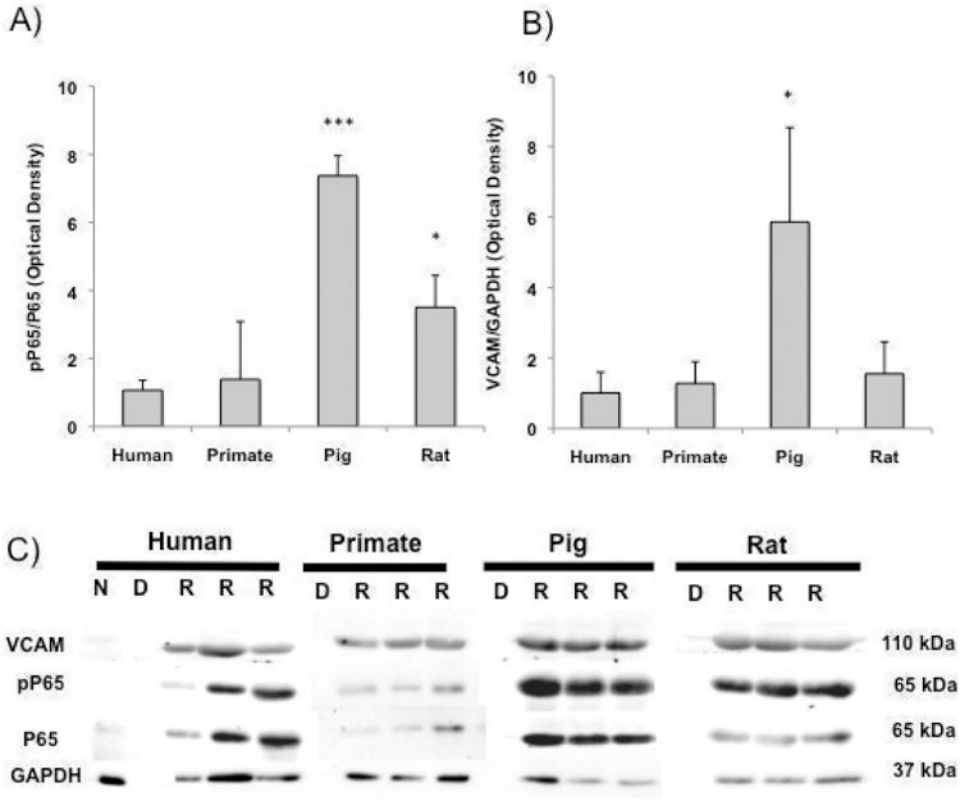

Figure 7. Scaffold species source dictates EC inflammatory response

A) pP65/P65 and B) VCAM/GAPDH presence ECs seeded onto human, primate, rat and pig tissue. C) Representative western blots of native 'N', decellularized 'D' and recellularized 'R' rat, pig, primate and human lung slices immunoblotted for phosphorolated P65 (relative to P65) and VCAM/GAPDH (n≥3). * indicates p≤ 0.05, *** indicates p≤ 0.001 relative to ECs on human tissue.